Gold Bull (2013) 46:267–274
DOI 10.1007/s13404-013-0114-9

ORIGINAL PAPER

Stimuli-responsive gold nanohybrids: chemical synthesis and electrostatic directed assembly on surfaces by AFM nanoxerography

Stéphane Lemonier · Pierre Moutet · Wissam Moussa · Mathias Destarac · Laurence Ressier · Jean-Daniel Marty

Published online: 13 November 2013

Abstract Stimuli-responsive nanohybrids based on gold nanoparticles coated with poly(acrylic acid) were synthesized. Their intrinsic properties (i.e., zeta potential and hydrodynamic diameter) were easily adjusted through the control of pH. This allows modulating the intensity of the electrophoretic forces exerted by charge patterns on the nanohybrids during the development step in AFM nanoxerography and controlling the directed assembly of nanohybrids onto charged patterns.

Keywords Nanohybrids · AFM nanoxerography · pH responsive · Directed assembly

Introduction

In recent years, there has been a considerable interest in the development of metal- and semiconductor-based colloidal nanoparticles (NPs). This interest arise first from their unique optical, electronic, and catalytic properties and also because nanometer-sized structures are appropriate for interfacing with biomacromolecules (proteins, DNA…) and probing intracellular environments [1]. These inorganic nanoparticles are usually coated with an organic or inorganic layer that provides solubility, long-term colloidal stability, and functionalization. These coated NPs, also called "nanohybrids", adopt some characteristics from the components that compose them; synergistic effects can also produce properties not present in any of the parts. Hence, a tremendous amount of studies has been performed, either to control the size and shape of the inorganic core and/or to choose the chemical structure of the stabilizing ligand shell. This allows tailoring NPs with specific properties for applications based on electron transfer (electronics, catalysis, electrochemistry, photochemistry) or lock–key interaction (recognition, sensorial operations,…) [2]. Among them, those which are able to respond to an external stimulus are referred to as "stimuli responsive." Different kinds of stimuli have been described in the literature: (1) physical stimuli: temperature, ionic strength, polarity of solvent, photochemical irradiation, electric or magnetic field, mechanical stress,…; (2) chemical stimuli: pH, specific complexation of ions, redox reactions,…; and (3) biochemical stimuli: DNA hybridization, enzyme/substrate complexes…. These responses are manifested as dramatic changes in the material properties, dimensions, structure, and interactions and may lead to their rearrangement or changes in their aggregation state. This could be taken in good account in an increasing number of applications. For instance, catalytic activity of nanohybrids dispersed in solution can be controlled by applying such a stimulus in order to induce either a change in the organic shell diffusion properties of the nanohybrids or a reversible aggregation useful for the recovering of the catalyst [3]. In biological applications, external stimuli allowed for instance the control of drug delivery for small drugs encapsulated inside those nanohybrids [1].

Additionally, during the past decade, a fascinating new challenge involving the spatially controlled arrangement of

Electronic supplementary material The online version of this article (doi:10.1007/s13404-013-0114-9) contains supplementary material, which is available to authorized users.

S. Lemonier · W. Moussa · J.-D. Marty (✉)
Laboratoire IMRCP, CNRS UMR 5623, Université de Toulouse, 118, route de Narbonne, 31062 Toulouse, France
e-mail: marty@chimie.ups-tlse.fr

P. Moutet · L. Ressier (✉)
LPCNO, INSA-UPS-CNRS, Université de Toulouse, 135 avenue de Rangueil, 31077 Toulouse Cedex 4, France
e-mail: laurence.ressier@insa-toulouse.fr

M. Destarac
Laboratoire HFA, CNRS UMR 5069, Université de Toulouse, 118, route de Narbonne, 31062 Toulouse, France

NPs, into two- or three-dimensional architectures has emerged. Depending on their final structure, these assemblies exhibit many interesting optical, magnetic, or conducting properties, paving the way to novel materials and applications [4–6]. Until now, different approaches based on the use of self-assembled systems [7–10], template effect [11, 12], or application of an external field (magnetic, electric, rheological,…) have been used to reach such a goal [13–15]. However, in order to successfully exploit NP assembly in the many foreseen applications and to ensure efficient scaling-up, a high level of direction and control is required. This necessitates having access to technology allowing formation of nanohybrid building blocks with controlled morphology and properties and to a controlled assembling process. In that context, the use of stimuli-responsive systems could be of special interest either to facilitate the assembly process or to modify the spatial arrangement of the assembled nanohybrids [16]. For instance, Mirkin and colleagues have obtained temperature-controlled organization of gold NPs by modifying them with DNA strands [17, 18]. Liquid crystalline thermotropic or lyotropic hybrid materials whose organization strongly depends on temperature or concentration have been also extensively studied [19–22].

Since the pioneering work of G. Decher on the assembly of organic compounds of opposite charges [12], the use of ionic interactions to direct the assembly of hybrid systems has attracted much attention. Hence, we have previously demonstrated that gold NPs covered with anionic or catanionic compounds can be selectively deposited on simple or complex pattern, bearing the opposite charge using AFM nanoxerography [3, 23]. We aim here to demonstrate and understand in which extent deposition of nanohybrids can be controlled by finely tuning the nanohybrid charge. For this, pH-responsive nanohybrids based on gold nanoparticles coated with poly(acrylic acid) (PAA) were synthesized. Fine adjustment of the zeta potential of these nanohybrids through pH was achieved to study the key parameters leading to the electrostatic directed assembly of gold nanohybrids on surfaces by AFM nanoxerography.

Experimental section

Reagents Tetrachloroauric acid trihydrate ($HAuCl_4 \cdot 3H_2O$), sodium citrate ($Na_3C_6H_5O_7$), acrylic acid (99 %), and sodium hydroxide (NaOH) were purchased from Aldrich Fine Chemicals and were used without further purification. The *O*-ethyl-*S*-(1-methoxycarbonyl) ethyldithiocarbonate MADIX agent (Rhodixan A1) was obtained from Rhodia and used as received. The 4,4′-azobis(4-cyanovaleric acid) (ACVA) initiator (>98 %) was purchased from Janssen Chimica and recrystallized from ethanol before use. Absolute ethanol (AnalaR normapur VWR) was used as received. Using a Purite device, water was purified through a filter and ion exchange resin (resistivity≈16 MΩ cm).

Characterization of polymer samples Average number molecular weights (M_n) and dispersities ($Đ$) were determined by size exclusion chromatography on an apparatus comprising a Varian ProStar 325 UV detector (dual wavelength analysis) and a Waters 410 refractive index detector, using two Shodex K-805L columns (8×300 mm, 13 μm). For PAA, a 0.1-mol L^{-1} $NaNO_3$ aqueous solution containing 100 ppm of NaN_3 was used as eluent, and the system was calibrated with narrow sodium poly(acrylate) standards ranging from 1,250 to 193,800 g mol^{-1}. ^1H NMR spectra were recorded on a Bruker ARX 400 at 400.13 MHz.

Dynamic light scattering (DLS) and zeta potential measurements were carried out at 25 °C with a Malvern Instrument Nano-ZS equipped with a He–Ne laser (λ = 633 nm). Samples were introduced into cells (pathway, 10 mm) after filtration through 0.45-μm PTFE micro-filters. The correlation function was analyzed via the nonnegative least square (NNLS) algorithm to obtain the distribution of diffusion coefficients (D) of the solutes, and then, the apparent equivalent hydrodynamic diameter ($<D_h>$) was determined using the Stokes–Einstein equation. Mean diameter values were obtained from three different runs. Standard deviations were evaluated from diameter distribution and were equal to 5 nm for all samples. For zeta potential measurements, zeta potential were extracted from mobility values using the Smoluchowski model.

Transmission electron microscopy A drop of the aqueous dispersions was placed on a carbon-coated copper transmission electron microscopy (TEM) grid and left to dry under air. For samples needing negative staining, the TEM grids were successively placed on a drop of the NP dispersion for 2 min, on a drop of an aqueous solution of uranyl acetate (2 wt%, 2 min), and finally, on a drop of distilled water, after which the grids were then air-dried before introduction into the electron microscope. The samples were observed with a HITACHI HU12 microscope operating at 70 kV. Size distribution was determined by manual counting on ca. 150 particles, using the WCIF Image J software.

UV–visible spectroscopy measurements An Analytik Jena diode array spectrometer (Specord 600) or a BMG Labtech diode array spectrometer (Spectrostar nano) equipped with a temperature control system was used for UV–visible absorption spectra recording (optical path length, 1 cm).

Polymer synthesis The typical procedure for synthesizing the RAFT/MADIX polymers of the study were as follows, with AA taken as an example: 7 mg of ACVA, 43 mg of Rhodixan A1, 5 g of acrylic acid, 4 g of ethanol, and 12.5 g of water were placed in a two-neck round-bottomed flask equipped with a magnetic stirrer and a reflux condenser. The solution was then degassed for 15 min by bubbling argon. It was then heated at 70 °C during 4 h, keeping a slow stream of argon in the

reactor. After this period of time, the solution was cooled down to ambient temperature, and the polymer was analyzed. AA conversion was >99 % (^{1}H NMR in D_2O). Dispersity value was determined by size exclusion chromatography in water equal to 1.7.

Formation of Au NPs with sodium citrate Spherical gold nanoparticles were prepared according to the following procedure: to 2 mL of a 1.10^{-2}-mol L^{-1} $HAuCl_4$ solution, 18 mL of distilled water was added [24]. This solution was boiled under stirring. Then 2 mL of a 38.8 10^{-3}-mol L^{-1} sodium citrate solution was added under reflux. The NP dispersion turned from yellow to dark, then red color in 10 min. The solution was then cooled down to room temperature.

Coating of preformed NPs and modification of pH Typically, for a final polymer concentration of $5{\cdot}10^{-4}$ wt%, 0.75 mL of a 10^{-3} wt% aqueous stock solution of PAA was added to 0.75 mL of aqueous gold NPs stock solution to yield coated NPs ($[Au(0)]_{final}$=4.5 10^{-4} mol L^{-1}). Nanohybrid dispersions were then centrifuged to remove excess of unbound organic species. Modification of pH values was performed by addition of small quantities of NaOH or HCl solutions.

AFM nanoxerography Charge writing was carried out into 100-nm thin films of 996,000 molecular weight poly(methyl methacrylate) (PMMA) spin-coated on *p*-doped (10^{16} cm^{-3}) silicon wafers. It was performed in air under ambient conditions, using a Multimode 8 atomic force microscope from Bruker. Charges were injected into the PMMA thin film by applying voltage pulses with an external generator to a conductive AFM tip. The *z*-feedback was adjusted to control the tip-sample distance during charge writing. The pulse length and the frequency of voltage pulses were fixed at 1 ms (long value compared to the cantilever oscillation period) and 50 Hz, respectively, while the pulse amplitude was fixed at ±80 V. The tip velocity was fixed at 10 μm/s for all experiments. These specific writing conditions were chosen regarding previous works because of their reliability and reproducibility, and this especially at such high voltages without tip and/or sample damaging [25]. Surface potential mappings of these charge patterns was carried out by the AFM-based electric technique of amplitude modulation Kelvin force microscopy (KFM), using a lift height of 20 nm and a scan rate of 0.5 Hz.

After charge writing, a two-stage development was performed [23]: a 30-μL drop of colloidal dispersion with desired pH was deposited on charge patterns for 30 s. pH adaptation from the original pH 5 solution was performed only few seconds prior to the drop in order to prevent agglomeration of the gold nanohybrids. After a 30-s rinsing in pure ethanol, delicate drying of the samples was achieved using a nitrogen steam.

The resulting nanohybrid assemblies were characterized by AFM topographical observations in tapping mode.

Results and discussion

Polymer synthesis

The precise control of the macromolecular characteristics is essential to better understand the role of the polymer in NP stabilization and surface modification. In the last years, RAFT/MADIX polymerization appeared as a method of choice to prepare well-defined water-soluble polymers whose molecular weights can be predicted from reactants stoichiometry [2, 26]. Moreover, this technique is highly tolerant to functional groups usually present in hydrophilic monomers, and it can be carried out in water or polar solvents. PAA is a well-known pH-responsive polymer, which can be easily prepared by RAFT/MADIX. Thus, PAA with a low molecular weight was synthesized by RAFT/MADIX polymerization mediated by the *O*-ethyl-*S*-(1-methoxycarbonyl)ethyl dithiocarbonate MADIX agent (Rhodixan A1). The conditions of reactions were chosen so that the targeted M_n was 10,000 g mol^{-1} [3]. Indeed, Schneider and Decher showed that the chain length is a crucial parameter for simultaneously avoiding flocculation while obtaining good rates of polyion deposition at the particle surface. Longer polymer chains will bridge and aggregate particles, whereas smaller ones will limit bridging flocculation [27]. Acrylic acid was polymerized in water at 70 °C with a minimum of ethanol to solubilize the hydrophobic Rhodixan A1, using 4′-azobis(4-cyanovaleric acid) as initiator. A monomer conversion greater than 99 % was achieved after 4 h of reaction. At this stage, the MADIX agent had fully reacted as shown by high-performance liquid chromatography (HPLC).

The M_n values of PAA estimated from SEC performed in DMF (with poly(methyl methacrylate) calibration) matched well those predetermined by the initial concentrations of both monomer and Rhodixan A1.

Synthesis and characterization of Au NPs modified with PAA

Citrate-stabilized gold nanoparticles were obtained through the Turkevitch reaction and the reduction of a $HAuCl_4{\cdot}3H_2O$ by sodium citrate [24]. Figure 1a, b shows TEM images and corresponding particle size histogram of the synthesized NPs. The NPs were approximately spherical and well dispersed. The mean particle diameter was 15.6 nm with a standard deviation of 4.0 nm. The nanoparticle dispersions obtained via this procedure exhibited a broad surface plasmon resonance absorption band around 520 nm, resulting in a pink–red color of the solutions. Negatively charge citrate species at the surface

of the nanoparticles induced a short-term stability of the Au NPs in water. Moreover, addition of HCl on those NPs induced their irreversible aggregation. Therefore, in order to obtain NPs with a tunable zeta potential, those pristine NPs were subsequently covered with PAA (see "Experimental section") using a "grafting to" approach. PAA have been often reported to act as efficient steric, electrostatic, and also electrosteric barriers against destabilization of aqueous dispersions of inorganic particles. Interaction of PAA with Au NPs was first evidenced by small changes in absorbance spectra. Indeed wavelength at maximum absorbance shifted from 522 for pristine Au NPs to 520 nm after modification with PAA polymer (see Figure S1 in electronic SUPPORTING INFORMATION). Moreover, Fig. 1c displays a typical image obtained after negative staining from Au@PAA$_{10k}$ dispersions. No bare NPs were observed. The nanohybrids clearly showed to have a core-shell morphology, the dark cores corresponding to the electron-dense Au atom embedded into a circular brighter thin polymer shell (lower than 2 nm in the dry state). The data collected confirm the adsorption of PAA on the surface of Au NPs. This adsorption may occur from interactions of either main carboxylic functions or dithiocarbonate terminal functions [2, 28].

The modifications of properties induced by a change of pH were then studied. In solution, PAA has good solubility at high pH values; however, it has poor solubility and even collapses, entangling together to precipitate from solution at low pH values (pH<4) in its acidic form. Although PAA has been extensively used to stabilize Au NPs, its pH-induced properties have not been thoroughly investigated [3]. When a PAA polymer layer is physically or chemically attached to the gold NP surface, not only a steric stability is acquired but also the properties of the Au NPs can be controlled to some extent in response to one of these small changes in the environmental parameters like pH. Due to their interaction with the inorganic surfaces, the mobility of PAA chains is restricted. For polymer segments close to the anchoring points, relatively higher energy input will be required to undergo transitions [2]. Nevertheless, far from the anchoring point, more space and free volume are available, providing energetically and spatially favorable conditions for rearrangement. Hence, any change of pH value will induce a modification of the ionic charges present on the surface of Au@PAA nanohybrids. The resulting modification of the hydrodynamic diameter and zeta potential of Au@PAA nanohybrids as a function of pH is depicted in Fig. 2a, b. At pH 2, nanohybrids have a zeta potential equal to −5±2 mV. Increasing the pH value up to 7.5 induces a decrease in zeta potential to −55±2 mV due to the deprotonation of the carboxylic groups of PAA. However, complete ionization on polyelectrolytes is certainly difficult to reach due to electrostatic effects exerted by other adjacent ionized groups, especially when considering this adsorbed polymer systems. We then studied the evolution of hydrodynamic diameter as a function of pH value. For pH values above 4, the hydrodynamic diameter was mainly affected by hybridization level of the nanohybrids. Hence, at pH 4.5, a hydrodynamic diameter of, i.e., 13±5 nm was observed in good agreement with the expected values from structural parameters of the nanohybrids. Upon ionization, the coiled chains extended responding to the electrostatic repulsions of the generated negative charges. As a result, the hydrodynamic diameter of nanohybrids slightly increased (up to 20 nm) at higher pH values. For low pH values (pH<4), NPs were covered by PAA in its carboxylic form. The lowering of repulsive interactions and the possibility of hydrogen bonding induced the formation of larger aggregates, which ultimately results in complete flocculation–decantation of the nanohybrids after a few hours. In order to avoid agglomeration of the gold nanohybrids during AFM nanoxerography (see "AFM nanoxerography"), pH adaptation from an original pH 5 solution was performed only few seconds prior to the nanohybrid assembly. In addition, the chemical modifications of the polymer shell resulted in the modification of the spectral properties of the nanohybrids as clearly observed in the UV–visible spectra. Apart from a decrease in intensity with time for low pH values (pH<3, see Figure S1 in electronic SUPPORTING INFORMATION), a slight decrease of lambda max was also observed by decreasing pH (Fig. 2c). Those nanohybrids were easily redispersed by increasing the pH to its initial value.

Thus, those nanohybrids present a negative effective surface charge that could be easily adjusted by controlling the pH value of the colloidal aqueous dispersion.

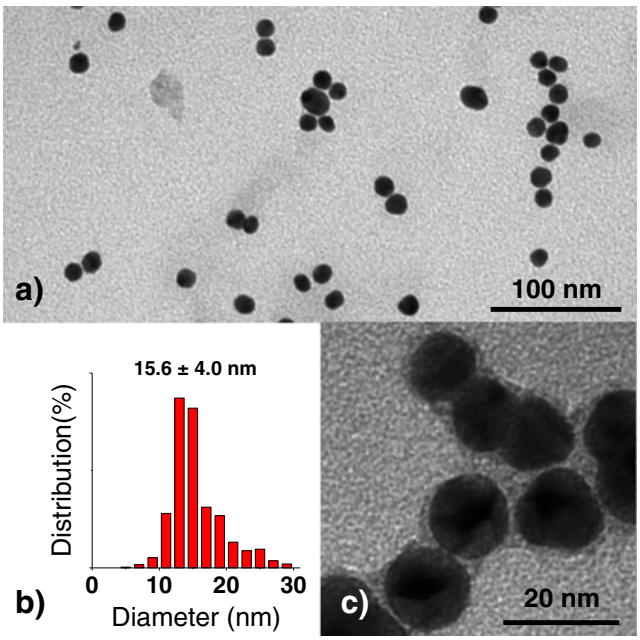

Fig. 1 **a** TEM image and **b** corresponding mean diameter distribution of Au NPs obtained by the Turkevitch method ; **c** TEM image of Au NPs subsequently covered with PAA polymer and negatively stained

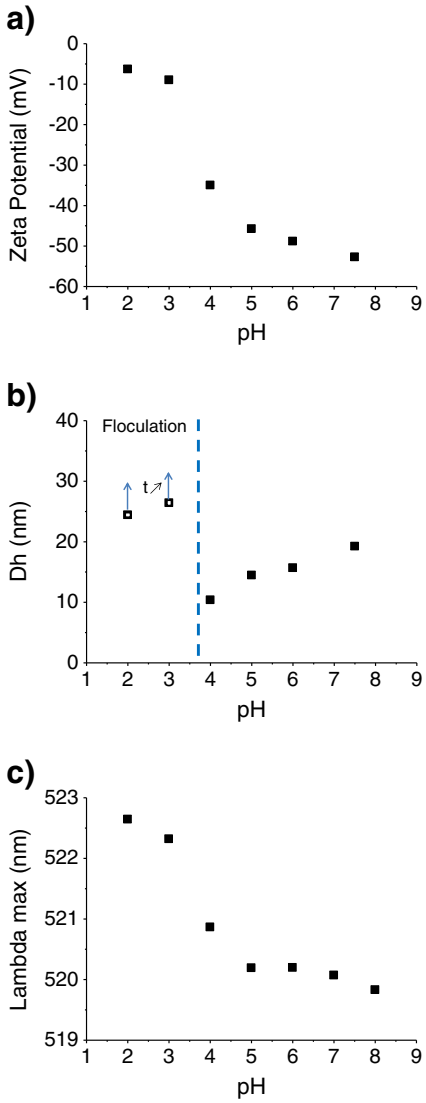

Fig. 2 Variation of zeta potential (**a**), hydrodynamic diameter Dh (**b**), and lambda max (**c**) as a function of pH for Au@PAA_{10k} nanohybrids ([Au(0)]=4.5.10^{-4} mol L^{-1}, [polymer]=5·10^{-4} wt%)

AFM nanoxerography

Over the past few years, nanoxerography by atomic force microscopy (AFM) has emerged as a versatile method for colloid assembly, directly from the bulk liquid phase onto solid templates [3, 23, 29–32]. This technique is a nanoscale adaptation of the industrial printing process of xerography. It uses the strong electric fields generated by charge patterns written into electret thin films to trap any charged and/or polarizable colloidal nanoparticles via electrostatic interactions. It requires neither expensive clean-room nor vacuum equipment.

In this work, we used the protocol of AFM nanoxerography that we developed in a previous work [23] to assemble Au nanohybrids from their aqueous dispersions (Fig. 3). The first step consists of writing charge patterns of desired polarity and geometry into a PMMA thin film through a polarized AFM tip. The second step consists of incubation of a drop of nanohybrid aqueous dispersion on the electrostatically patterned substrates followed by immersion into pure ethanol. The samples are finally dried under nitrogen flow in order to remove any traces of solvent.

During this development step, two electrostatic forces, generated by the local electric field E created by charge patterns, act on the nanohybrids: the electrophoretic forces and the dielectrophoretic forces.

The electrophoretic forces describe the Coulomb interaction between the effective charge of the nanohybrids dispersed in solution and the electric field E generated by the charge patterns. They can be expressed by the Eq. (1):

$$\boldsymbol{F}_{EP} = Q_{\mathrm{ef}}\boldsymbol{E} \tag{1}$$

where Q_{ef} is the effective charge of the nanohybrids dispersed in solution. These forces cause nanohybrids carrying an effective surface charge to be attracted toward the charge patterns of opposite polarity and repelled away from the charge patterns of same polarity. The dielectrophoretic forces arise from the interaction of the nonuniform electric E generated by the charge patterns and the dipole induced by E in the nanohybrids by distortion of the electrical double layer around them. For a spherical nanohybrid of radius R, in a suspending solvent with a relative permittivity ε_s, the dielectrophoretic forces can be expressed by the Eq. (2) [33]:

$$\boldsymbol{F}_{DEP} = 2\pi \mathrm{R}^3 \varepsilon_s \varepsilon_0 \,\mathrm{Re}[K]\nabla \boldsymbol{E}^2 \tag{2}$$

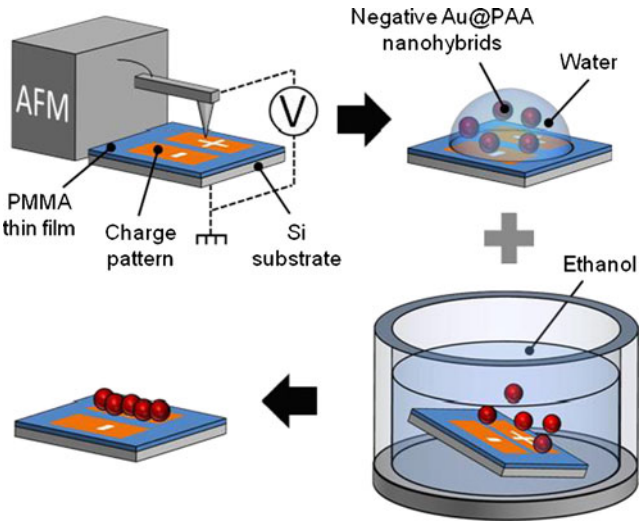

Fig. 3 Principle of AFM nanoxerography

where Re [K] is the real part of the Clausius–Mossotti factor K, given by:

$$K = \frac{\varepsilon^*_{NH} - \varepsilon^*_S}{\varepsilon^*_{NH} + 2\varepsilon^*_S} \quad (3)$$

with ε^*_{NH} and ε^*_S the complex permittivities of the nanohybrids and the suspending solvent, respectively. The dielectrophoretic forces are independent of the effective charge of the nanohybrids. They cause nanohybrids which are more polarizable than their solvent to be attracted toward the charge patterns of both polarities.

Figure 4a presents a typical KFM image of two 5×10-μm rectangular charge patterns of opposite polarity written by AFM in a 100-nm PMMA thin film. As shown on the KFM cross sections, their surface potential is about ±7 V. Figure 2b shows typical AFM topographical images of the resulting directed assembly of gold nanohybrids on charge patterns similar to those presented in Fig. 2a, for various pH of the colloidal dispersions.

At pH 5, these observations revealed that gold nanohybrids were massively grafted on the positively charged rectangle into a compact monolayer and strongly repelled from the negative one (a depletion zone is observed on the negatively charged pattern). In this case, the nanohybrids, presenting a strong negative zeta potential of (−50 mV) (Fig. 4b), were driven by the predominant electrophoretic forces. These forces attracted the negatively charged nanohybrids toward the charge pattern of opposite polarity and repelled them from the charge pattern of same polarity. The dielectrophoretic forces, attractive for charge patterns of both polarities since the nanohybrids are more polarizable than the aqueous solvent, were weak compared to the electrophoretic forces. They contributed for a small part to the directed assembly of nanohybrids on the positive pattern but were not sufficient to counterbalance the repulsive electrophoretic forces on the negative charge pattern.

At pH 4, nanohybrids were selectively assembled on the positive rectangle with a lower density, without any repulsion by the negative one. In that case, the combination of the attractive electrophoretic and dielectrophoretic forces on nanohybrids resulted in their directed assembly on the positive pattern, even if the electrophoretic forces were weaker than in the previous case due to the smaller zeta potential in absolute

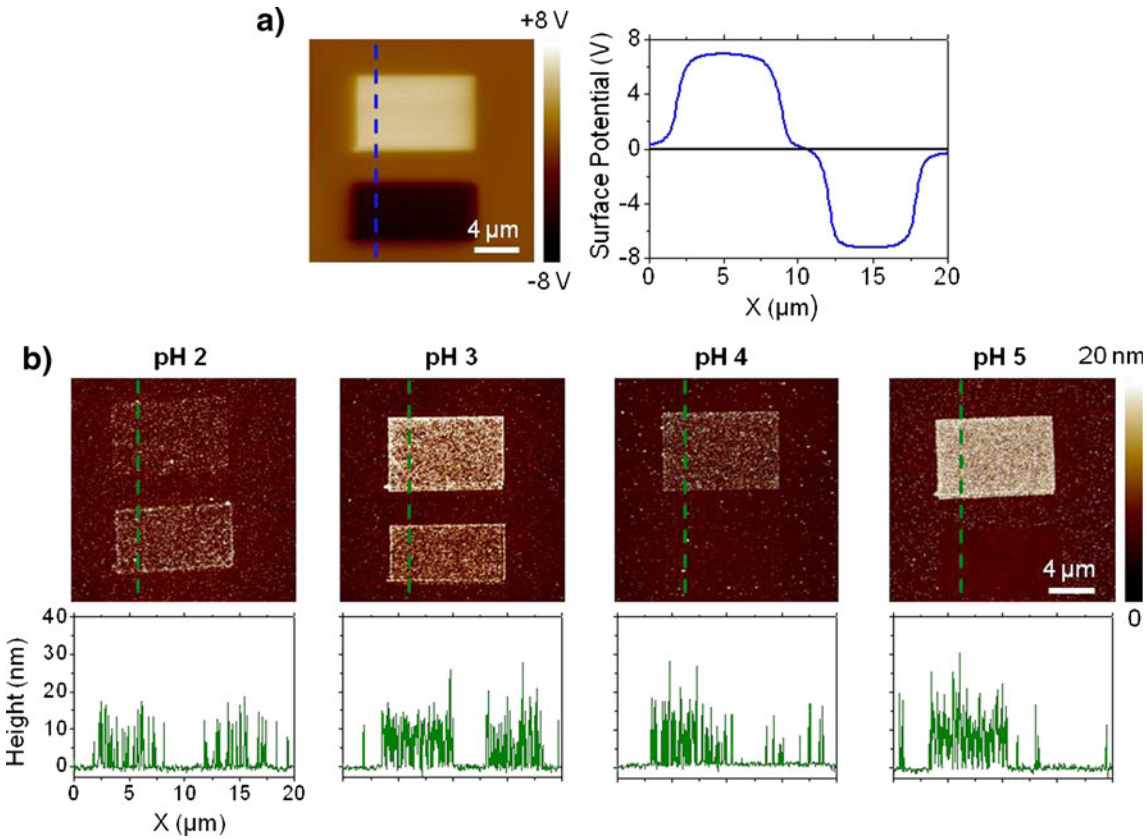

Fig. 4 **a** KFM surface potential image and associated section of rectangular charge patterns (the *bright pattern* is positively charged, the *dark one* is negatively charged) written by AFM in a 100-nm PMMA thin film, **b** AFM topographical images and associated sections of the resulting directed assembly of Au@PAA nanohybrids on charge patterns similar to those presented in (**a**), for different pHs of the colloidal dispersions N.B: from repeated experiments, the density of nanoparticles could not be regarded as significantly different on pattern of opposite charge at pH 2

value (−35 mV) of nanohybrids at this pH. However, the repulsive electrophoretic forces generated by the negative charge pattern were not strong enough in that case to overcome the attractive dielectrophoretic and nonselective forces acting on nanohybrids, resulting into a nonspecific absorption of nanohybrids on the negatively charged pattern.

At pH 3 and pH 2, selective assembly of nanohybrids occurred on both positive and negative charge patterns with similar nanohybrid density, indicating that the directed assembly of nanohybrids was only governed by the attractive dielectrophoresis forces. The effective charge of nanohybrids was too weak at these pH (zeta potential below −10 mV) to induce significant electrophoretic forces. For all pH, it is to note that the directed assemblies of gold nanohybrids were dense enough to be visible by optical microscopy. Very few particles were adsorbed outside the charge patterns.

These results clearly demonstrate that the fine tuning of the effective charge of Au@PAA nanohybrids through pH modulation of the colloidal dispersion allows controlling the intensity of the electrophoretic forces exerted by charge patterns on the nanohybrids during the development step. This offers the opportunity to drive the directed assembly of nanohybrids onto positively charged patterns only or on charge patterns of both polarities.

Conclusion

Stimuli-responsive nanohybrids based on gold nanoparticles coated with PAA were synthesized. Their intrinsic properties (i.e., zeta potential and hydrodynamic diameter) were easily adjusted through the control of pH. This allows modulating the intensity of the electrophoretic forces exerted by charge patterns on the nanohybrids during the development step in AFM nanoxerography and controlling the directed assembly of nanohybrids onto charged patterns.

Acknowledgments The authors thank the CMEAB for TEM facilities and Juliette Fitremann and Etienne Palleau for fruitful discussions.

References

1. Beija M, Salvayre R, Lauth-de Viguerie N, Marty JD (2012) Colloidal systems for drug delivery: from design to therapy. Trends Biotechnol 30(9):485–496. doi:10.1016/j.tibtech.2012.04.008
2. Beija M, Marty JD, Destarac M (2011) RAFT/MADIX polymers for the preparation of polymer/inorganic nanohybrids. Prog Polym Sci 36(7):845–886. doi:10.1016/j.progpolymsci.2011.01.002
3. Beija M, Palleau E, Sistach S, Zhao XG, Ressier L, Mingotaud C, Destarac M, Marty JD (2010) Control of the catalytic properties and directed assembly on surfaces of MADIX/RAFT polymer-coated gold nanoparticles by tuning polymeric shell charge. J Mater Chem 20(42):9433–9442. doi:10.1039/c0jm01781g
4. Cheon J, Park JI, Choi JS, Jun YW, Kim S, Kim MG, Kim YM, Kim YJ (2006) Magnetic superlattices and their nanoscale phase transition effects. Proc Natl Acad Sci U S A 103(9):3023–3027. doi:10.1073/pnas.0508877103
5. Collier CP, Vossmeyer T, Heath JR (1998) Nanocrystal superlattices. Annu Rev Phys Chem 49:371–404. doi:10.1146/annurev.physchem.49.1.371
6. Zhuang JQ, Shaller AD, Lynch J, Wu HM, Chen O, Li ADQ, Cao YC (2009) Cylindrical superparticles from semiconductor nanorods. J Am Chem Soc 131(17):6084. doi:10.1021/ja9015183
7. Klein J, Kumacheva E, Mahalu D, Perahia D, Fetters LJ (1994) Reduction of frictional forces between solid-surfaces bearing polymer brushes. Nature 370(6491):634–636. doi:10.1038/370634a0
8. McMillan RA, Paavola CD, Howard J, Chan SL, Zaluzec NJ, Trent JD (2002) Ordered nanoparticle arrays formed on engineered chaperonin protein templates. Nat Mater 1(4):247–252. doi:10.1038/nmat775
9. Nie ZH, Fava D, Kumacheva E, Zou S, Walker GC, Rubinstein M (2007) Self-assembly of metal-polymer analogues of amphiphilic triblock copolymers. Nat Mater 6(8):609–614. doi:10.1038/nmat1954
10. Park S, Lim JH, Chung SW, Mirkin CA (2004) Self-assembly of mesoscopic metal-polymer amphiphiles. Science 303(5656):348–351. doi:10.1126/science.1093276
11. Gavioli L, Cavaliere E, Agnoli S, Barcaro G, Fortunelli A, Granozzi G (2011) Template-assisted assembly of transition metal nanoparticles on oxide ultrathin films. Prog Surf Sci 86(3–4):59–81. doi:10.1016/j.progsurf.2011.02.001
12. Decher G (1997) Fuzzy nanoassemblies: toward layered polymeric multicomposites. Science 277(5330):1232–1237. doi:10.1126/science.277.5330.1232
13. Gao Y, Tang ZY (2011) Design and application of inorganic nanoparticle superstructures: current status and future challenges. Small 7(15):2133–2146. doi:10.1002/smll.201100474
14. Mann S (2009) Self-assembly and transformation of hybrid nano-objects and nanostructures under equilibrium and non-equilibrium conditions. Nat Mater 8(10):781–792. doi:10.1038/nmat2496
15. Min YJ, Akbulut M, Kristiansen K, Golan Y, Israelachvili J (2008) The role of interparticle and external forces in nanoparticle assembly. Nat Mater 7(7):527–538. doi:10.1038/nmat2206
16. Karg M, Hellweg T, Mulvaney P (2011) Self-assembly of tunable nanocrystal superlattices using poly-(NIPAM) spacers. Adv Funct Mater 21(24):4668–4676. doi:10.1002/adfm.201101115
17. Macfarlane RJ, Lee B, Jones MR, Harris N, Schatz GC, Mirkin CA (2011) Nanoparticle superlattice engineering with DNA. Science 334(6053):204–208. doi:10.1126/science.1210493
18. Rosi NL, Mirkin CA (2005) Nanostructures in biodiagnostics. Chem Rev 105(4):1547–1562. doi:10.1021/cr030067f
19. Hegmann T, Qi H, Marx VM (2007) Nanoparticles in liquid crystals: synthesis, self-assembly, defect formation and potential applications. J Inorg Organomet Polym Mater 17(3):483–508. doi:10.1007/s10904-007-9140-5
20. Mitov M, Bourgerette C, de Guerville F (2004) Fingerprint patterning of solid nanoparticles embedded in a cholesteric liquid crystal. J Physics-Condens Mat 16(19):S1981–S1988. doi:10.1088/0953-8984/16/19/010
21. Saliba S, Davidson P, Imperor-Clerc M, Mingotaud C, Kahn ML, Marty JD (2011) Facile direct synthesis of ZnO nanoparticles within lyotropic liquid crystals: towards organized hybrid materials. J Mater Chem 21(45):18191–18194. doi:10.1039/c1jm13253a

22. Saliba S, Mingotaud C, Kahn ML, Marty JD (2013) Liquid crystalline thermotropic and lyotropic nanohybrids. Nanoscale 5(15):6641–6. doi:10.1039/C3NR01175E
23. Palleau E, Sangeetha NM, Viau G, Marty JD, Ressier L (2011) Coulomb force directed single and binary assembly of nanoparticles from aqueous dispersions by AFM nanoxerography. Acs Nano 5(5): 4228–4235. doi:10.1021/nn2011893
24. Rahme K, Gauffre F, Marty JD, Payre B, Mingotaud C (2007) A systematic study of the stabilization in water of gold nanoparticles by poly(ethylene oxide)-poly(propylene oxide)-poly(ethylene oxide) triblock copolymers. J Phys Chem C 111(20):7273–7279. doi:10.1021/jp070274+
25. Ressier L, Le Nader V (2008) Electrostatic nanopatterning of PMMA by AFM charge writing for directed nano-assembly. Nanotechnology 19(13):135301. doi:10.1088/0957-4484/19/13/135301
26. Boyer C, Stenzel MH, Davis TP (2011) Building nanostructures using RAFT polymerization. J Polym Sci Polym Chem 49(3):551–595. doi:10.1002/pola.24482
27. Schneider G, Decher G (2008) Functional core/shell nanoparticles via layer-by-layer assembly. investigation of the experimental parameters for controlling particle aggregation and for enhancing dispersion stability. Langmuir 24(5):1778–1789. doi:10.1021/la7021837
28. Glaria A, Beija M, Bordes R, Destarac M, Marty JD (2013) Understanding the role of ω-end groups and molecular weight in the interaction of PNIPAM with gold surfaces. Chem Mater 25: 1465–2004. doi:10.1021/cm400480p
29. Palleau E, Sangeetha NM, Ressier L (2011) Quantification of the electrostatic forces involved in the directed assembly of colloidal nanoparticles by AFM nanoxerography. Nanotechnology 22(32): 325603. doi:10.1088/0957-4484/22/32/325603
30. Ressier L, Palleau E, Garcia C, Viau G, Viallet B (2009) How to control AFM nanoxerography for the templated monolayered assembly of 2 nm colloidal gold nanoparticles. Ieee T Nanotechnol 8(4):487–491. doi:10.1109/tnano.2009.2016089
31. Seemann L, Stemmer A, Naujoks N (2007) Selective deposition of functionalized nano-objects by nanoxerography. Microelectron Eng 84(5–8):1423–1426. doi:10.1016/j.mee.2007.01.108
32. Tzeng SD, Lin KJ, Hu JC, Chen LJ, Gwo S (2006) Templated self-assembly of colloidal nanoparticles controlled by electrostatic nanopatterning on a Si3N4/SiO2/Si electret. Adv Mater 18(9):1147. doi:10.1002/adma.200501542
33. Jones TB (1995) Electromechanics of particles. Cambridge University Press, Cambridge